Turkish Journal of Chemistry

http://journals.tubitak.gov.tr/chem/

Research Article

Turk J Chem
(2017) 41: 967 – 986

doi:10.3906/kim-1703-72

Adsorption of copper ions and alizarin red S from aqueous solutions onto a polymeric nanocomposite in single and binary systems

Omnia ALI*, Sahar MOHAMED
Department of Chemistry, Faculty of Science, Helwan University, Ain Helwan, Cairo, Egypt

Received: 29.03.2017 • **Accepted/Published Online:** 23.06.2017 • **Final Version:** 20.12.2017

Abstract: Adsorption of Cu(II) ions and alizarin red S (ARS) has been studied using beads of chitosan (CS) and a chitosan/ZnO nanorod composite (CS-ZnO) in single and binary systems. The beads were synthesized and characterized using Fourier transform infrared spectroscopy, X-ray diffraction, high-resolution transmission electron microscopy, scanning electron microscopy, and energy dispersive X-ray analysis. Factors affecting adsorption of Cu(II) ions and ARS such as pH and initial concentrations as well as adsorption kinetics, isotherms, thermodynamics, reusability, and competitive adsorption in binary systems were studied. The results showed that the adsorption kinetics and isotherm data for both adsorbates followed a pseudo-second-order model and the Freundlich model, respectively. Studies of intraparticle diffusion and Dumwald–Wagner models indicated that the adsorption occurred in a complex mechanism where the intraparticle diffusion stage was not the only rate-determining step for both adsorbates. Thermodynamic studies showed that the adsorption process was favorable, endothermic, and physisorptive in nature. In both single and binary systems, CS-ZnO beads showed better adsorption efficiency than CS beads. For the binary system, Cu(II) ions did not affect the adsorption of ARS; however, ARS reduced the Cu(II) adsorption.

Key words: Cu(II) ions, alizarin red S, nanocomposite, adsorption, reusability, binary system

1. Introduction

Most industries, such as textile, dye, plastic, paper, and electroplating, discharge effluents containing toxic dyes and heavy metals, which might be very dangerous to humans and the environment.[1,2] Transfer of heavy metals from contaminated water to soil results in the accumulation of these heavy metals in living plants, and then these heavy metals are transferred to humans via the food chain. Because of their nonbiodegradable nature, heavy metals tend to accumulate in the human body and can cause serious health disorders.[3] Copper is one of the most dangerous heavy metals because it is highly toxic even if it exists in low concentrations in water or soil.[4] For example, Cu-contaminated soils planted with tomato produce tomatoes with Cu ion contents ranging from 32.9 to 1696.5 mg kg^{-1}.[5] Higher levels of Cu(II) ions can cause serious toxicological concerns, such as vomiting, cramps, convulsions, or even death.[6]

Huge quantities of the dyes are annually produced worldwide and the effluents of textile and dyestuff industries are the two main sources for dye-polluted wastewater.[7] The release of untreated dye wastewater threatens environmental safety by posing color pollution and serious hazards to aquatic organisms. In addition, dye-polluted wastewater is difficult to treat effectively when it contains high salt-like, recalcitrant dyes that are

*Correspondence: omniaibrahim95@gmail.com

resistant to biodegradation processes by microorganisms.[8] The removal of dyes from wastewater is a challenge due to their high stability towards oxidizing agents, light, and heat. Alizarin red S (ARS) is an anionic dye that is used in the textile industry for dyeing cotton, wool, and woven fabrics. Due to its complex structure, ARS is highly durable and difficult to degrade; in addition, it has carcinogenic effects and causes environmental problems. Only a few studies were reported on adsorption of ARS from wastewater.[9−11]

There are numerous methods established for removing dyes and heavy metals from water, such as ion exchange, chemical precipitation, photocatalysis, membrane filtration, and adsorption.[12] Since many of these methods are expensive when applied on a large scale, adsorption is considered as the most powerful and popular technique used to treat wastewater from contamination. Among the different adsorbents, polymeric adsorbents as polysaccharides are effective environmentally safe adsorbents. Incorporation of nanoparticles into the polymeric matrix produces nanocomposites with improved efficiency for removal of many pollutants. Polysaccharides and polysaccharides' nanocomposites have been extensively studied for removal of dyes and heavy metals, e.g., guar gum,[13] cellulose,[14] starch,[15,16] and chitosan.[17] Chitosan is a natural linear polysaccharide, with free amine and hydroxyl groups that make it suitable for adsorption of both metals and dyes.[18] Due to their biocompatibility, biodegradability, nontoxicity, and high sorption capacities, nanoparticle-impregnated chitosan seems to be a promising adsorbent for water treatment. In recent years, different chitosan composites such as chitosan/TiO_2,[19,20] chitosan/TiO_2/CdS,[21] chitosan/alumina,[22] chitosan/CuO,[23] and chitosan/graphene oxide[24,25] were studied for water treatment processes.

ZnO is a cheap environmentally friendly material and its surface has many functional groups, such as hydroxyl groups, which can be active sites for adsorption.[26,27] ZnO nanoparticles are applied in solar energy conversion, luminescence, photocatalysis, electrostatic dissipative coating, transparent UV protection films, and chemical sensors.

Water has always been regarded as the most strategic of raw materials; however, Egypt suffers from water pollution due to nonstop release of wastewater into the Nile River.[28] Moreover, the river receives large discharges of organic pollutants and heavy metals from industrial activities in the Greater Cairo region. The aim of the present work was to explore and extend the applications of chitosan/ZnO composite to remove ARS and copper ions from aqueous solutions in single and binary systems. In addition, the aim was to optimize the maximum adsorption efficiency of the synthesized nanocomposite. Kinetics, equilibrium, and thermodynamics of the adsorption for ARS and copper ions using chitosan and a chitosan/ZnO nanorod composite (CS-ZnO) were investigated. Moreover, reusability studies of adsorbents for both pollutants have also been investigated.

2. Results and discussion

2.1. Characterization

2.1.1. X-ray diffraction (XRD)

XRD was carried out to investigate the immobilization of n-ZnO onto CS. Figure 1 shows the XRD patterns of the n-ZnO and CS-ZnO nanocomposite beads, where the broad peak at 20.01° revealed that CS is amorphous in nature.[29] The XRD pattern of the ZnO powder shows the peaks at 2θ values of 31.72°, 34.38°, 36.21°, 47.51°, 56.56°, 62.82°, 67.9°, and 69.07°, which correspond to the crystal planes of (1 0 0), (0 0 2), (1 0 1), (1 0 2), (1 1 0), (1 0 3), (1 1 2), and (2 0 1), respectively, of the crystalline ZnO.[30] In the XRD pattern of the CS-ZnO sample, the peaks at 2θ values of 31.70°, 34.41°, 36.24°, 47.57°, 56.49°, 62.95°, 68.05°, and 69.11° correspond to the crystal planes of (1 0 0), (0 0 2), (1 0 1), (1 0 2), (1 1 0), (1 0 3), (1 1 2), and (2 0 1), respectively, of the crystalline ZnO. All the diffraction peaks are in good agreement with those of the hexagonal

wurtzite structure of ZnO (JCPDS card 36–1451).[31] The results revealed the successful impregnation of n-ZnO onto CS.

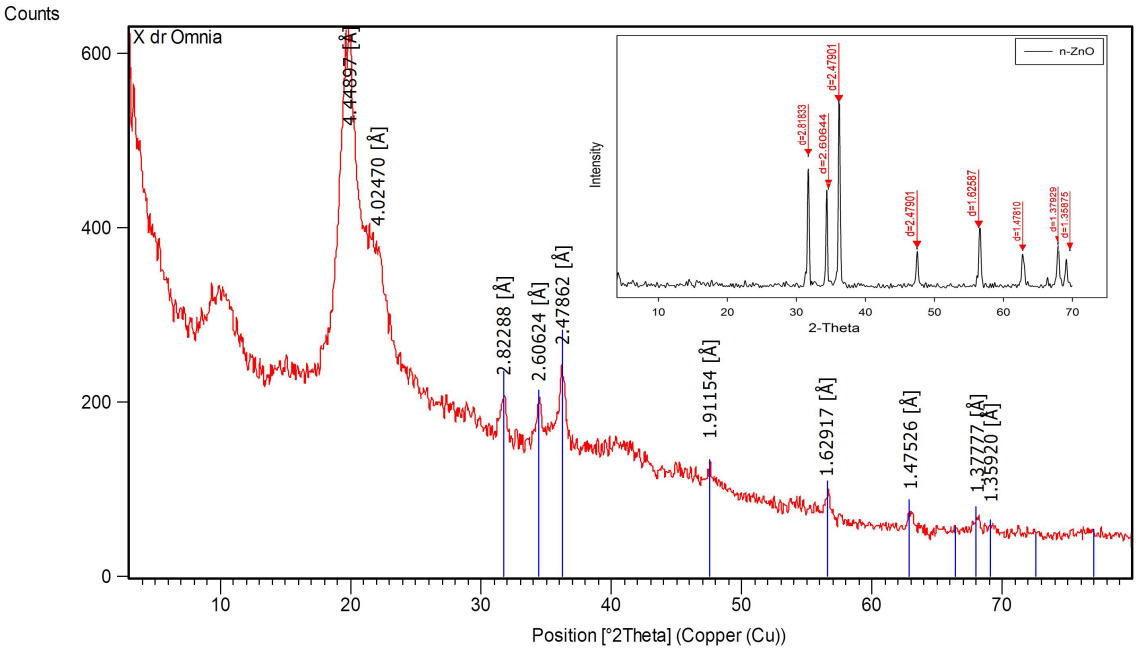

Figure 1. XRD pattern of CS-ZnO. The inset shows the XRD pattern of n-ZnO.

2.1.2. Fourier transform infrared (FTIR) spectroscopy

FTIR spectra of CS and CS-ZnO beads are shown in Figure 2. It is clear that the characteristic peaks of the chitosan polymer appeared in both samples.[32] The peak at 3459 cm^{-1} corresponded to the stretching vibration of –OH and $–NH_2$.[29] However, some differences were detected where a peak assigned at 1090 cm^{-1} in the CS sample (vibration and stretching of C–N bond and C–O bond)[30,33] weakened and shifted to 1020 cm^{-1} in the case of CS-ZnO. This was probably due to the formation of a coordination bond with ZnO. A new band assigned at 438 cm^{-1} in the case of the CS-ZnO spectrum confirmed the existence of n-ZnO.[34]

2.1.3. Scanning electron microscopy (SEM) and energy dispersive X-ray analysis (EDAX)

SEM images of CS-ZnO are shown in Figure 3. As seen in Figure 3a, the image revealed the rough homogeneous surface of the sample. The EDAX spectrum is shown in Figure 3b. The spectrum displayed peaks of zinc and oxygen in the synthesized CS-ZnO beads, confirming that n-ZnO was successfully impregnated homogeneously in the synthesized beads. Figures 3c and 3d show the surface morphology of CS-ZnO beads after adsorption of ARS and Cu, respectively; clusters of ZnO appeared at the surface as white areas. Figure 3e represents the mapping results of Cu and Zn in Cs-ZnO after adsorption of Cu(II). This image confirms the uniform distribution of ZnO particles in the polymeric matrix as well as the uniform adsorption of Cu(II) ions.

2.1.4. High-resolution transmission electron microscopy (HR-TEM)

Figure 4 demonstrates HR-TEM photographs of CS-ZnO nanocomposite beads. The images showed that ZnO existed in the form of nanorods with average lengths of 40–71 nm and diameters of 3.3–7 nm.

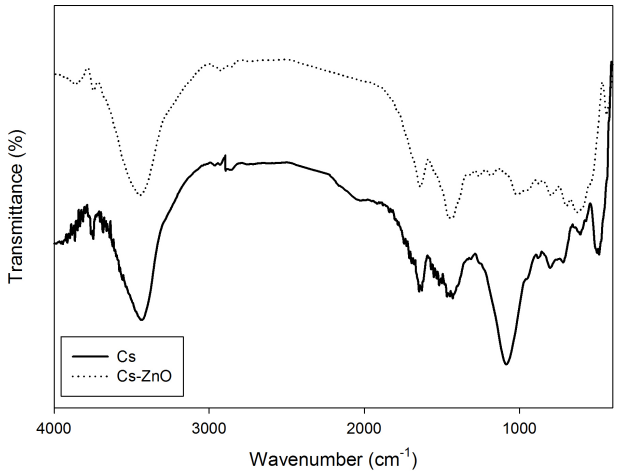

Figure 2. FTIR spectra of CS and CS-ZnO.

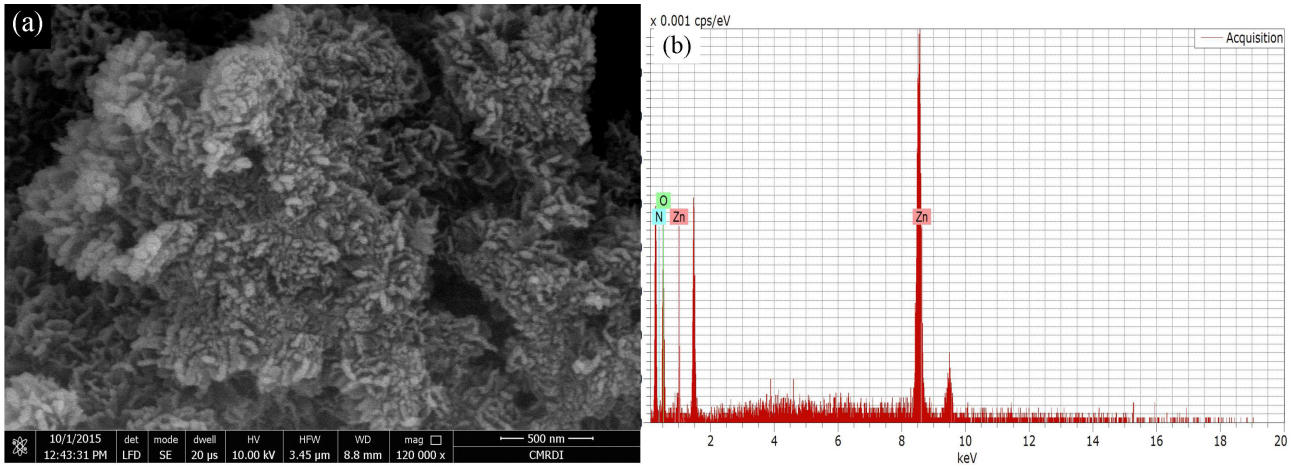

Figure 3. (a) SEM image, (b) EDAX spectrum of CS-ZnO, (c) CS-ZnO after adsorption of ARS, (d) CS-ZnO after adsorption of Cu(II), (e) mapping result of CS-ZnO after adsorption of Cu(II).

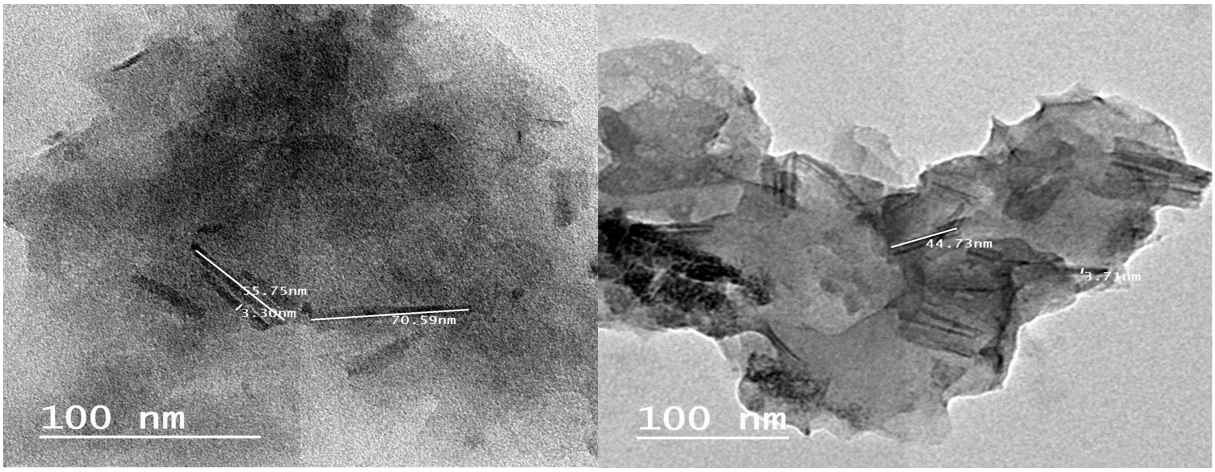

Figure 4. HR-TEM images of CS-ZnO.

The results of XRD patterns, FTIR spectra, and EDAX spectra along with HR-TEM images confirmed that the n-ZnO-impregnated chitosan beads were successfully synthesized.

2.2. Adsorption studies

2.2.1. Effect of initial pH

The effect of pH on the adsorption was studied by soaking 0.1 g of CS or CS-ZnO for 48 h at 25 °C in a solution of 10 mg L^{-1} Cu(II) or 20 mg L^{-1} ARS. As shown in Figure 5a, the uptake of Cu(II) was affected by the pH of the solution. For both samples, as pH increased, the Cu(II) adsorption increased. In the case of CS-ZnO, the adsorption efficiency reached the maximum value at pH 6.

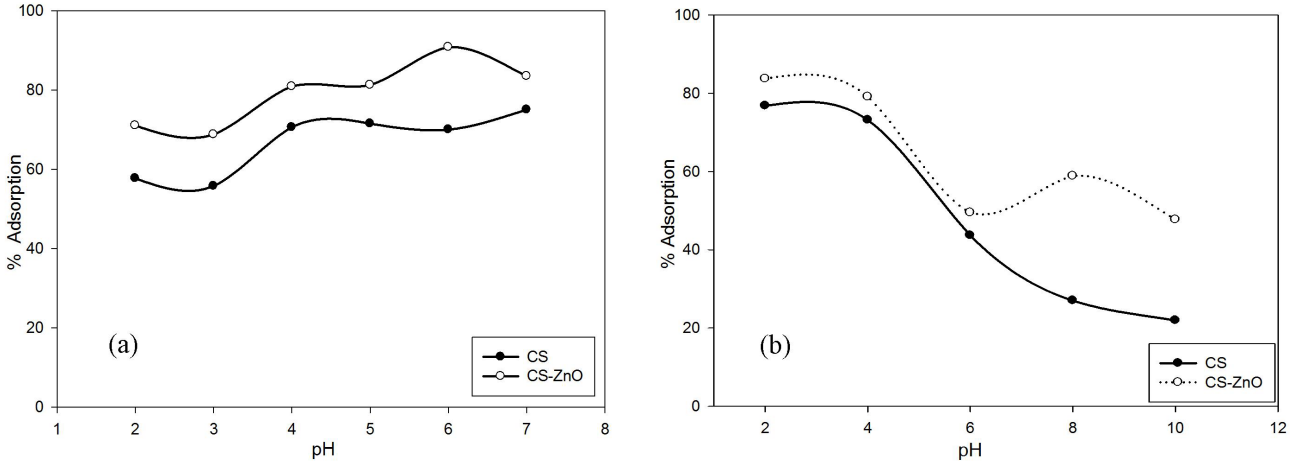

Figure 5. Effect of pH on % of adsorption of CS and CS-ZnO for (a) [Cu(II)] = 10 mg L^{-1} and (b) [ARS] = 20 mg L^{-1}, 25 °C, 48 h.

For ARS (Figure 5b), it was observed that both adsorbents showed a better adsorption capacity at lower pH values. The dye uptake increased as pH decreased and the removal efficiency was maximum at a solution pH of 2. It is worth mentioning that the increased % of adsorption of ARS at pH 8 was attributed to the presence of n-ZnO. Joshi and Shrivastava[35] reported similar results in the case of adsorption of ARS using ZnO. For further experiments, pH 6 and 2 were selected for Cu(II) and ARS, respectively.

2.2.2. Effect of contact time

The effect of contact time on the % of adsorption of Cu(II) and ARS onto adsorbents was studied and the results are shown in Figures 6a and 6b. The figure shows that the contact time necessary to reach saturation is greater than 24 h for Cu(II) and 27 h for ARS. It was observed that CS-ZnO showed a higher % of adsorption than CS for both Cu(II) and ARS. At the early stages, the rate of adsorption was high due to more available vacant sites and high concentration gradient between the adsorbate in aqueous and solid adsorbent surfaces. At later stages, the concentration gradient was reduced, which resulted in decreasing the rate of adsorption until equilibrium.[36]

2.2.3. Effect of initial concentration

The effect of initial concentration of Cu(II) and ARS on the adsorption capacity (q_e) of CS and CS-ZnO is shown in Figures 7a and 7b. It is obvious that as the initial concentration increased from 10 to 100 mg L^{-1}, the

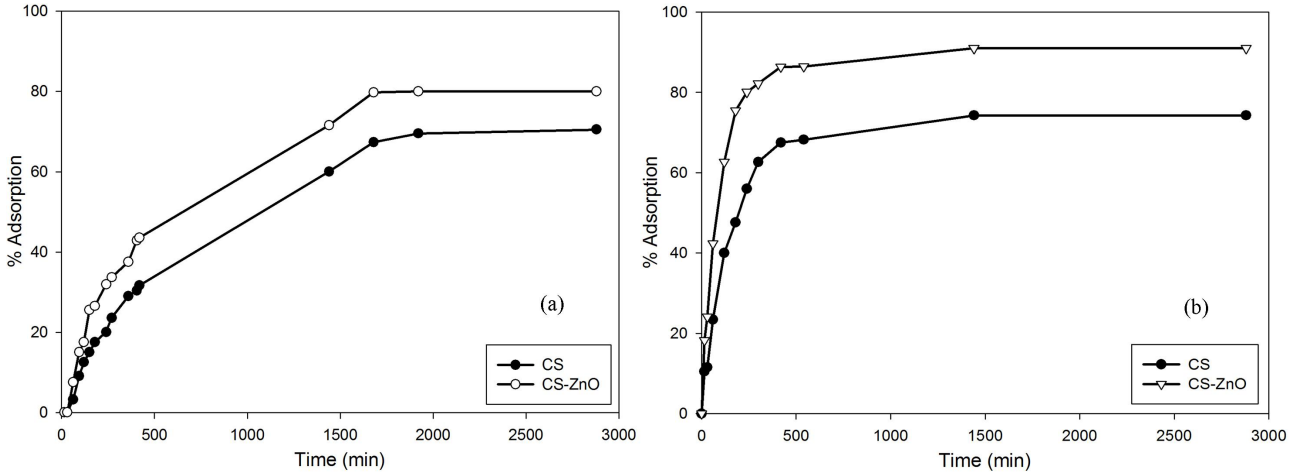

Figure 6. Effect of contact time on % of adsorption of CS and CS-ZnO for (a) [Cu(II)] = 10 mg L^{-1} at pH 6 and (b) [ARS] = 20 mg L^{-1} at pH 2, 25 °C, 48 h.

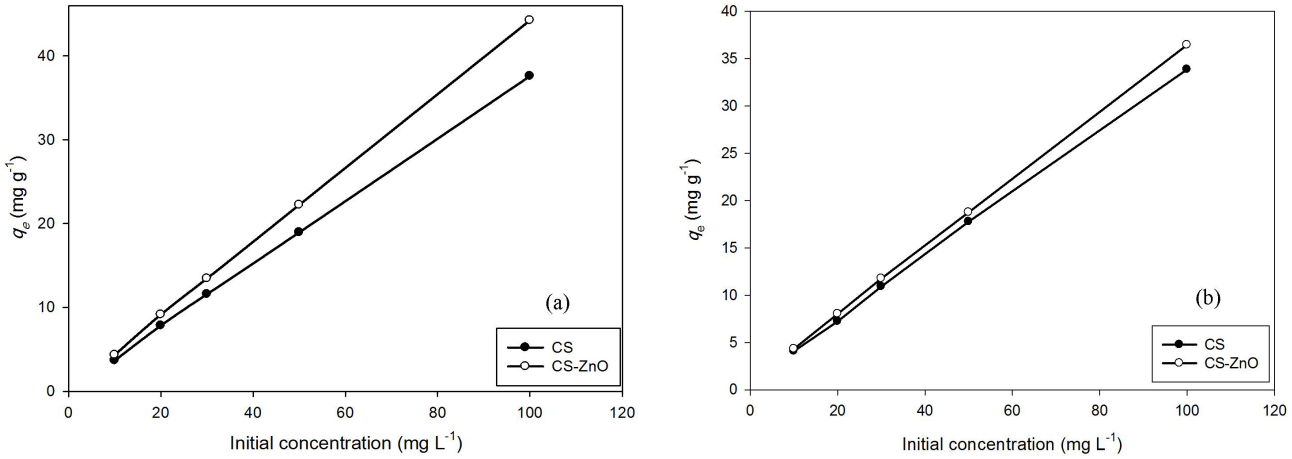

Figure 7. Effect of initial concentration on the adsorption capacity of CS and CS-ZnO for (a) Cu(II) at pH 6 and (b) ARS at pH 2, 25 °C, 48 h.

experimental adsorption capacity, q_e, increased from 4.33 to 44.24 and from 4.32 to 36.43 mg g^{-1} for Cu(II) and ARS, respectively. These results emphasize that increasing the initial concentration of pollutants supplies the driving force required to enhance the mass transfer between the solution and adsorbent.

2.3. Adsorption kinetics

To understand the kinetics of the adsorption process for both pollutants, the results were examined using the well-known pseudo-first-order, pseudo-second-order, Elovich, intraparticle diffusion, and Dumwald–Wagner models.

2.3.1. Pseudo-first-order model

Lagergren's equation of the pseudo-first-order model is widely used to describe the kinetics of the adsorption process as follows:

$$\log(q_e - q_t) = \log q_e - \left(\frac{k_1 t}{2.303}\right), \tag{1}$$

where q_e and q_t are the adsorbed concentration of adsorbate (mg g^{-1}) at equilibrium and at any time t, respectively, and $k_1(min^{-1})$ is the rate constant of first-order adsorption. The slope of the plot of log $(q_e - q_t)$ as a function of t can be used to determine the first-order rate constant k_1.

2.3.2. Pseudo-second-order model

The pseudo-second-order equation based on adsorption equilibrium capacity may be expressed in the following form:

$$\frac{t}{q_t} = \frac{1}{k_2 q_e^2} + \frac{t}{q_e}, \tag{2}$$

where k_2 is the rate constant of the second-order adsorption (g mg^{-1} min^{-1}).

Similarly, the slope of the plot of t/q_t as a function of t was used to determine the second-order rate constant k_2.

2.3.3. Elovich model

The Elovich model equation is a rate equation that describes chemisorption on energetically heterogeneous solid surfaces.[37] This model is usually reliable with systems in which the equilibrium adsorption isotherm is described by the Temkin model.[38] It can be expressed as follows:

$$q_t = \frac{1}{b}\ln(ab) + \frac{1}{b}\ln(t), \tag{3}$$

where a is the initial adsorption rate (mg g^{-1} min^{-1}), and the parameter *1/b* (mg g^{-1}) is related to the number of sites available for adsorption. If this model fits the experimental results, plotting q_t versus *ln (t)* should give a straight line.

Table 1 shows the different parameters obtained from the three employed kinetics models. As illustrated in the table, the values of correlation coefficients (R^2) for the pseudo-second-order model were the highest, indicating that the experimental data correlated well with that model. This conclusion was also confirmed by the low values of the total mean error ($\epsilon\%$). The calculated q_e values obtained from the pseudo-first-order model were not reasonable values since they were much lower than experimental q_e values. On the other hand, the calculated q_e values of the pseudo-second-order model were found to be closer to the experimental ones. These results suggest that the adsorption process is pseudo-second-order, where the adsorption of either Cu(II) or ARS takes place on an energetically heterogeneous surface.

The rate constant (K_2) values for CS-ZnO were higher than that of CS for both pollutants, which indicates that the adsorption rate was higher in the case of CS-ZnO than that of CS.

Although the adsorption kinetics were well described by the pseudo-second-order model, the Elovich model (properly fits chemisorption processes) was not compatible with the experimental data. This observation was confirmed by the low values of total mean error ($\epsilon\%$). These results suggest that the adsorption is physisorptive in nature. Similar results were reported by Giraldo et al.[39]

Table 1. Calculated parameters of the pseudo-first-order, pseudo-second-order, Elovich, and Dumwald–Wagner models for adsorption of Cu(II) and ARS onto CS and CS-ZnO beads.

Pseudo-first-order						
Adsorbate	Adsorbent	Experimental q_e (mg g^{-1})	q_e (mg g^{-1})	$K_1 \times 10^3$ (min^{-1})	R^2	ε %
Cu(II)	CS	3.01	1.48	4.61	0.9335	23.19
	CS-ZnO	3.69	1.37	12.44	0.7951	37.56
ARS	CS	7.06	2.40	1.38	0.9633	5.51
	CS-ZnO	8.01	2.70	2.30	0.8411	18.17
Pseudo-second-order						
Adsorbate	Adsorbent	Experimental q_e (mg g^{-1})	q_e (mg g^{-1})	K_2 (g mg^{-1} min^{-1})	R^2	ε %
Cu(II)	CS	3.01	3.18	0.46	0.9988	2.40
	CS-ZnO	3.69	3.79	2.05	0.9992	2.23
ARS	CS	7.06	8.96	0.95	0.9985	1.82
	CS-ZnO	8.01	9.32	1.75	0.9986	2.25
Elovich model						
Adsorbate	Adsorbent	Experimental q_e (mg g^{-1})	a (mg g^{-1} min^{-1})	$1/b$ (mg g^{-1})	R^2	ε%
Cu(II)	CS	3.01	0.08	0.68	0.9311	7.15
	CS-ZnO	3.69	0.21	0.74	0.8640	16.48
ARS	CS	7.06	0.04	1.49	0.9207	20.16
	CS-ZnO	8.01	0.05	1.73	0.9640	10.20
Dumwald–Wagner model						
Adsorbate	Adsorbent	B(min^{-1})	Intercept	R^2	ε %	
Cu(II)	CS	0.0070	0.0298	0.9958	4.53	
	CS-ZnO	0.0120	0.1247	0.9850	7.14	
ARS	CS	0.0013	0.0138	0.9954	6.71	
	CS-ZnO	0.0016	0.0787	0.9847	9.36	

2.4. Adsorption mechanism

Since pseudo-first-order, pseudo-second-order, and Elovich models do not suggest a definite mechanism for adsorption, the results were analyzed using the intraparticle diffusion and Dumwald–Wagner models to predict the rate-limiting step. There might be one or more controlling steps for the adsorption process such as external diffusion, pore diffusion, surface diffusion, and adsorption on the pore surface, or a combination of more than one step. In their model, Weber and Morris[40] assumed that the initial rate of intraparticle diffusion is calculated by the following equation:

$$q_t = k_i t^{1/2} + C, \tag{4}$$

where k_i is the intraparticle diffusion rate constant (mg g^{-1} min$^{-1/2}$) and C (mg g^{-1}) is a constant related to the thickness of the boundary layer; as the boundary layer effect increases, the value of C increases. If the intraparticle diffusion is the rate-determining step for the adsorption process, a plot of q_t against the square

root of time ($t^{1/2}$) gives a straight line that passes through the origin. If the line does not pass through the origin, then the intraparticle diffusion is not the rate-limiting step, but it is still involved in the adsorption process.[41] However, if the plot exhibits two or more intersecting lines, then two or more stages control the adsorption process.[42]

The Dumwald–Wagner model was established as a successful model for different adsorption systems and it is expressed as:[39]

$$\ln(1 - \frac{q_t}{q_e}) = Bt, \tag{5}$$

where B is the film diffusion rate ($\min^{-1}$). Plotting $\ln(1 - (q_t / q_e))$ versus time gives a straight line and if it passes through the origin, then intraparticle diffusion is the rate-limiting step; otherwise, the rate-limiting step is film diffusion. Furthermore, the higher intercept value reflects the greater effect of the film diffusion step on the rate of adsorption.[43]

Figures 8a and 8b show the intraparticle diffusion model where q_t is plotted versus time $t^{1/2}$ for ARS and Cu(II) ion adsorption. It is clear that the plots are not linear over the whole time range, which revealed that the adsorption process was not controlled by one step. Fitting of the intraparticle model for ARS (Figure 8a) exhibits three intersecting lines for each adsorbent. The first and the second lines are related to the surface adsorption and intraparticle diffusion, respectively. The third line represents the final equilibrium stage at which the intraparticle diffusion started to slow down due to the extremely low adsorbate concentration left in the solution.[44] The deviation of the straight line from the origin suggests that intraparticle diffusion was not the only rate-controlling step and the adsorption occurred through a complex mechanism. In the case of Cu(II) adsorption (Figure 8b), two intersecting sharp lines were obtained. The first line represents the rapid surface adsorption, while the second line indicates the intraparticle diffusion stage.

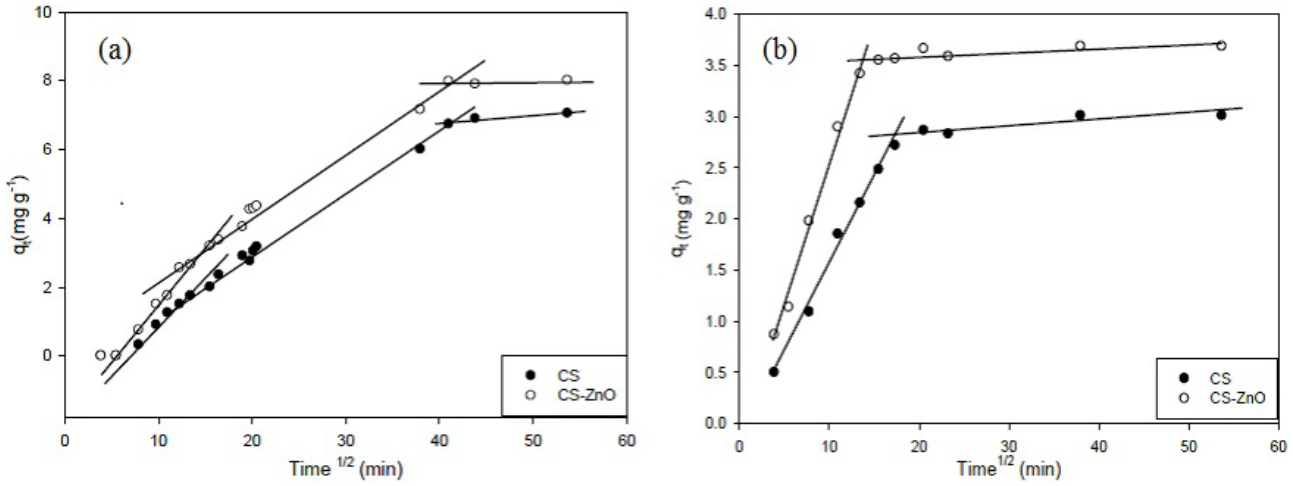

Figure 8. Intraparticle diffusion plots for adsorption of (a) [ARS] = 20 mg L^{-1} at pH 2 and (b) [Cu(II)] = 10 mg L^{-1} at pH 6, 25 °C, 48 h.

Dumwald–Wagner model parameters are shown in Table 1. As shown, the straight line did not pass through the origin, which confirmed that intraparticle diffusion is not the rate-limiting step and the film diffusion step controls the rate of adsorption process. The intercept values of Cs-ZnO are greater than those of Cs for both pollutants, which indicates that the film diffusion step has a greater effect in the case of Cs-ZnO. These

results confirmed the complex mechanism of adsorption where both intraparticle diffusion and film diffusion are involved.

2.5. Adsorption isotherms

The results of adsorption studies of Cu(II) and ARS at different concentrations ranging from 10 to 100 mg L^{-1} onto 0.1 g of adsorbent were expressed by four of the most popular employed equilibrium models: the Freundlich, Langmuir, Temkin and Dubinin–Radusckevisch–Kanager models.

2.5.1. Langmuir isotherm

The Langmuir model assumes monolayer adsorption where adsorption can take place on a fixed number of active sites disregarding the lateral interaction and steric limitations between the adjacent adsorbed species.[45] This model implies homogeneous adsorption where all active sites have the same energy and the same affinity toward the adsorbate particles,[46] and it is mainly applied to chemisorption system.[47] The mathematical expression for the linear form of Langmuir model is:

$$\frac{C_e}{q_e} = \frac{1}{bQ_e} + \frac{C_e}{Q_e}, \tag{6}$$

where q_e and C_e are the equilibrium adsorbate concentration in adsorbent (mg g^{-1}) and aqueous solution (mg L^{-1}), respectively. Q_e is the maximum adsorption capacity (mg g^{-1}) and b is the Langmuir constant related to the adsorption energy (L mg^{-1}).

2.5.2. Freundlich isotherm

The Freundlich adsorption isotherm[48] assumes a multilayer adsorption mechanism that takes place on a heterogeneous surface, where the adsorption capacity increases as the adsorbate concentration increases. The model assumes that the heterogeneous surface shows nonuniform distribution of adsorption heat and affinities and the adsorption heat is exponentially decreased upon the completion of adsorption process.[49] The model is described as follows:

$$\log q_e = \log k_f + \frac{1}{n} \log C_e, \tag{7}$$

where q_e and C_e are the same as in Langmuir model, k_f is the Freundlich constant related to the adsorption capacity [mg g^{-1} (mg $L^{-1})^n$], and n is an empirical parameter representing the energetic heterogeneity of the adsorption sites (dimensionless). The slope $(1/n)$ ranges between 0 and 1 and it is a measure of surface heterogeneity, where the more heterogeneous the surface is, the closer the *1/n* value is to zero.[46]

2.5.3. Temkin isotherm

This model postulates that the heat of adsorption of all molecules would decrease with increasing surface coverage linearly despite being exponential in the Freundlich equation. The Temkin isotherm is given by the following equation:[50]

$$q_e = k_1 \ln(k_2) + k_1 \ln C_e, \tag{8}$$

where q_e and C_e are the same as in the other models. k_1 and k_2 are Temkin constants, where k_1 is related to the heat of adsorption (J mol^{-1}) and k_2 is the equilibrium binding constant (L g^{-1}). Plotting q_e versus ln C_e gives a straight line from which k_1 and k_2 can be estimated.

2.5.4. Dubinin–Radusckevisch–Kanager isotherm

Experimental data were further analyzed by the Dubinin–Radushkevich model to identify whether the nature of the adsorption process was chemisorptive or physisorptive. In general, this model is compatible with adsorption processes on heterogeneous surfaces with a Gaussian energy distribution. The linearized form of this model is expressed as follows:

$$\ln q_e = \ln q_{(D-R)} - \beta\varepsilon^2, \tag{9}$$

$$\varepsilon = RT\ln(1 + \frac{1}{C_e}), \tag{10}$$

$$E = \frac{1}{\sqrt{2\beta}}, \tag{11}$$

where q_e and C_e are the same as in the Langmuir model, $q_{(D-R)}$ is the theoretical adsorption capacity (mg g^{-1}), β is a constant related to adsorption energy for a mole of the adsorbate (mol^2 kJ^{-2}), and R is Polanyi's potential. R is the ideal gas constant (0.008314 kJ K^{-1} mol^{-1}) and T is the absolute temperature (K). E (kJ mol^{-1}) is the mean free energy per molecule of adsorbate when it transfers from the bulk of the solution (infinity) to the adsorbent surface. The value of E reflects the nature of the adsorption process, where it is physisorptive if E $<$ 8 kJ mol^{-1} and chemisorptive if E lies between 8 and 16 kJ mol^{-1}.[51]

Table 2 shows the corresponding Langmuir, Freundlich, Temkin, and Dubinin–Radusckevisch–Kanager constants, error analysis values, and correlation coefficients. It can be concluded that the data were better fitted to the Freundlich model, since correlation coefficients for Cu(II) ions or ARS were close to unity. Error analysis values also confirmed the fitting of the Freundlich model to the experimental data and this suggested that the adsorption of both pollutants was physical in nature.[52] For Cu(II) ions or ARS adsorption on CS and CS-ZnO, $1/n$ values range between 0 and 1, which again indicates the surface heterogeneity of the adsorbents. The values of $1/n$ for CS-ZnO were lower than those of CS samples for both pollutants, confirming the more heterogeneous surface of the CS-ZnO sample. CS-ZnO samples showed higher values for k_f, which agree with the results of adsorption kinetics, since the adsorption capacity of CS-ZnO was greater than that of CS samples for both pollutants.

According to the Dubinin–Radushkevich model, the calculated value of E was much lower than 8 kJ mol^{-1}, which revealed that the adsorption for Cu(II) and ARS is physisorptive in nature.

2.6. Thermodynamics studies

The influence of temperature on the adsorption process was examined at temperatures of 298, 308, 318, 328, and 338 K for Cu(II) ions at pH 6 for 6 h and 293, 303, 308, 313, and 318 K for ARS at pH 2 for 7 h.

The equilibrium constant is temperature-dependent and it can be used to find the spontaneity and heat of the adsorption process. Presuming that the activity coefficients are unity at low concentrations (Henry's

Table 2. Calculated parameters of the Langmuir, Freundlich, Temkin, and D-R models for adsorption of Cu(II) and ARS onto CS and CS-ZnO beads.

Langmuir model					
Adsorbate	Adsorbent	b (L mg^{-1})	$q_{\max}$ (mg g^{-1})	R^2	ε %
Cu(II)	CS	0.004	500.00	0.7198	2.79
	CS-ZnO	0.015	333.33	0.6103	3.31
ARS	CS	0.011	133.33	0.7387	4.61
	CS-ZnO	0.019	111.11	0.8424	5.38
Freundlich model					
Adsorbate	Adsorbent	K_f (mg g^{-1} (mg L^{-1})^n)	$1/n$	R^2	ε % 7
Cu(II)	CS	1.25	0.99	0.9955	1.89 7
	CS-ZnO	1.94	0.97	0.9908	2.35 7
ARS	CS	1.27	0.87	0.9971	1.40 7
	CS-ZnO	1.46	0.84	0.9985	1.02 7
Temkin model					
Adsorbate	Adsorbent	k_1 (J mol^{-1})	k_2 (L g^{-1})	R^2	ε %
Cu(II)	CS	14.42	0.42	0.9178	20.27
	CS-ZnO	16.81	0.97	0.9239	18.77
ARS	CS	11.99	0.39	0.8950	22.56
	CS-ZnO	12.45	0.51	0.8984	21.24
D-R model					
Adsorbate	Adsorbent	E (kJ mol^{-1})	$q_{(D-R)}$ (mg g^{-1})	R^2	ε %
Cu(II)	CS	0.4918	16.32	0.9206	7.07
	CS-ZnO	0.9172	20.85	0.9507	5.30
ARS	CS	0.5128	13.61	0.8168	9.11
	CS-ZnO	0.5993	15.33	0.8866	7.34

law), the equilibrium constant can be calculated according to the following equation:

$$K_d = \frac{q_e}{C_e}. \tag{12}$$

The thermodynamic parameters, enthalpy change (ΔH), entropy change (ΔS), and Gibbs energy change (ΔG) can be calculated using the Van't Hoff equation:

$$\Delta G = -RT \ln K_d, \tag{13}$$

$$\ln K_d = \frac{\Delta S}{R} - \frac{\Delta H}{RT}, \tag{14}$$

where q_e and C_e are the equilibrium adsorbate concentrations in adsorbent (mg g^{-1}) and aqueous solution (mg L^{-1}), respectively. T is the temperature in Kelvin and R is the universal gas constant (8.314 J K^{-1} mol^{-1}). ΔH and ΔS were calculated from the slope and intercept of the plot of $\ln K_d$ versus *1/T*. ΔG for

each temperature was calculated using Eq. (13). All the thermodynamic parameters were estimated and are listed in Table 3. It was found that the R^2 values of the linear fitting lines were between 0.959 and 0.998, indicating that the values of enthalpy and entropy calculated for both adsorbents were confident.

Table 3. Thermodynamic data for the adsorption of Cu(II) ions and ARS onto CS and CS-ZnO beads.

Adsorbate	T (K)	CS			
		ln K_d	ΔG (kJ mol^{-1})	ΔH (kJ mol^{-1})	ΔS (J mol^{-1} K^{-1})
Cu(II)	298	0.03	–0.063	14.29	48.01
	308	0.18	–0.448		
	318	0.33	–0.880		
	328	0.56	–1.541		
	338	0.69	–1.925		
	T (K)	CS-ZnO			
		ln K_d	ΔG (kJ mol^{-1})	ΔH (kJ mol^{-1})	ΔS (J mol^{-1} K^{-1})
	298	1.14	–2.603	20.24	78.13
	308	1.61	–3.673		
	318	1.75	–3.971		
	328	1.95	–4.438		
	338	2.18	–4.952		
ARS	T (K)	CS			
		ln K_d	ΔG (kJ mol^{-1})	ΔH (kJ mol^{-1})	ΔS (J mol^{-1} K^{-1})
	298	–1.96	4.782	32.90	95.36
	308	–1.67	4.197		
	318	–1.38	3.539		
	328	–1.23	3.188		
	338	–0.87	2.311		
	T (K)	CS-ZnO			
		ln K_d	ΔG (kJ mol^{-1})	ΔH (kJ mol^{-1})	ΔS (J mol^{-1} K^{-1})
	298	–1.68	4.023	37.23	112.49
	308	–1.33	3.178		
	318	–1.06	2.520		
	328	–0.84	1.986		
	338	–0.44	1.034		

For adsorption of Cu(II) ions, the positive values of ΔH indicated that the adsorption process was endothermic in nature. The positive values for ΔS revealed the increasing randomness at the solid–solution interface; thus, the adsorption was favorable.[53] The negative values of ΔG suggested that the adsorption of Cu(II) ions was spontaneous. Increasing the temperature from 298 to 338 K resulted in more negative ΔG values for CS and CS-ZnO. These results reveal that increasing the temperature enhances the adsorption process.

In the case of adsorption of ARS, the positive values of ΔH and ΔS indicated that the adsorption process was endothermic in nature and favorable. However, the positive values of ΔG suggested that the adsorption of ARS was nonspontaneous in the temperature range of 298–318 K. These results indicated that the adsorption process belongs to the category of reactions that become favored above a definite temperature.[54]

The type of adsorbate–adsorbent interaction can be classified, to a certain extent, by the value of enthalpy change. ΔH in a physisorption process, such as van der Waals or electrostatic interaction, is lower than 80 kJ mol^{-1}, and for ΔH values higher than 80 kJ mol^{-1}, the interaction is chemisorption.[36] As illustrated in Table 3, ΔH values were lower than 80 kJ mol^{-1}, which confirmed that the adsorption process for both Cu(II) ions and ARS onto CS and CS-ZnO was physisorption.

The CS-ZnO sample showed greater values for ΔS, which revealed that the adsorption process resulted in more randomness and was more favorable than that for the CS sample.

2.7. Desorption and reusability studies

Recovery of pollutants from adsorbents has economic feasibility for adsorbent reusability. This relies on the adsorbent regeneration during successful consecutive adsorption/desorption cycles.

Desorption studies revealed complete regeneration of ARS using 0.5 M NaOH and partial regeneration for Cu(II) using 1 g L^{-1} EDTA. The adsorption-desorption for ARS was carried out successfully up to five cycles, where the adsorption efficiency of the fifth cycle was 51% for CS and 54% for CS-ZnO, while the desorption efficiency was 72% for CS and 84% for CS-ZnO. In the case of Cu(II) ions, the desorption efficiency for the first cycle was 52% for CS and 56% for CS-ZnO. However, the desorption efficiency of Cu(II) decreased dramatically in the subsequent cycles.

2.8. Binary system studies

In this work, the simultaneous adsorption of pollutants in the binary metal-dye system has been considered, since the two types (inorganic and organic pollutants) may be present in industrial wastewater. For comparison, the adsorption of both adsorbates was studied at pH 2 and 6 using a mixture of 10 mg L^{-1} Cu(II) and 20 mg L^{-1} ARS. The preliminary experiments showed that optimum adsorption capacities were achieved at pH 2 for both adsorbates. Thus, pH 2 was selected for adsorption studies for mixtures of [10, 20, 30, 50 and 100 mg L^{-1} ARS / 10 mg L^{-1} Cu(II)] at 20 °C for 48 h and the results are shown in Figures 9a–9d. Figures 9a and 9b illustrate that the presence of Cu(II) ions did not significantly affect the ARS adsorption. At the same time, as the initial concentration of ARS increased, the adsorption of Cu(II) ions decreased, which confirmed that the beads under investigation had a higher affinity for ARS than Cu(II) in the binary systems (Figures 9c and 9d).

2.9. Comparison with other studies

To explore the efficiency of the synthesized samples, the adsorption capacities of Cu(II) and ARS on the synthesized chitosan/ZnO nanorod composite were compared with other studies. As shown in Table 4, the adsorption capacity of Cu(II) that was obtained in the current work was higher than that obtained by chitosan in prawn shell[55] and lower than the other adsorbents. For ARS adsorption, adsorption capacity was also much higher than that obtained by biosorbent of *Lantana camara*[11] and it was comparable to the value obtained by n-Fe_3O_4-corn cover composite.[56] Moreover, to the knowledge of the authors, there have been no studies done for the simultaneous removal of Cu(II) and ARS in a binary system using the chitosan/ZnO nanorods composite. Accordingly, the synthesized nanocomposite could successfully be applied for the simultaneous removal of Cu(II) and ARS.

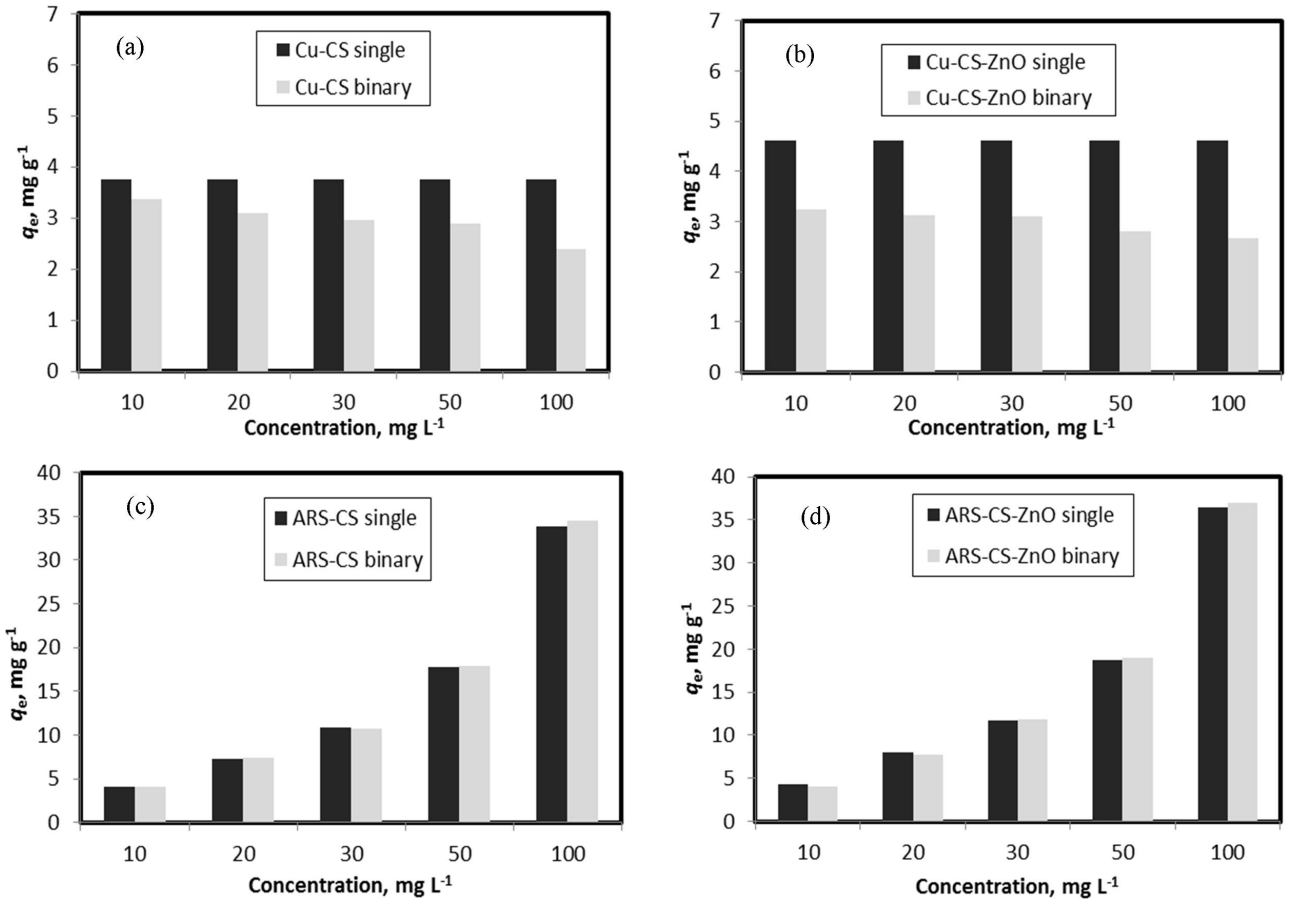

Figure 9. Adsorption capacity in single and binary systems for (a) Cu(II) onto CS, (b) Cu(II) onto CS-ZnO, (c) ARS onto CS, and (d) ARS onto CS-ZnO.

Table 4. Comparison of the adsorption efficiency of synthesized Cs-ZnO with other adsorbents for the adsorption of Cu(II) and ARS.

Adsorbents for Cu(II)	q_{max} (mg g^{-1})	Reference	Adsorbents for ARS	q_{max} (mg g^{-1})	Reference
Konjac glucomannan-poly(acrylic acid) hydrogel	27.17	[61]	Biosorbent of *Lantana camara*	1.17	[11]
Chitosan-coated sand	8.18	[62]	Graphene oxide	88.50	[63]
Chitosan in prawn shell	0.73	[55]	Magnetic chitosan	40.12	[10]
Chitosan-coated bentonite	12.14	[64]	Activated clay modified by iron oxide	32.70	[65]
Functionalized activated carbon	54.00	[66]	n-Fe_3O_4-corn cover composite	10.75	[56]
Chitosan/ZnO nanorods composite	3.69	Present study	Chitosan/ZnO nanorods composite	8.01	Present study

2.10. Conclusions

Cu(II) and ARS have been successfully removed from aqueous solutions using chitosan and a chitosan/ZnO nanorod composite in single and binary systems. The characterization of the synthesized adsorbents by XRD,

FTIR, and EDAX along with HR-TEM demonstrated that chitosan beads impregnated with ZnO nanorods were successfully synthesized. Adsorption kinetics of Cu(II) and ARS onto the studied adsorbents could be described by the pseudo-second-order model. The experimental data fit the Freundlich isotherm model well. The calculated thermodynamic parameters indicated that the adsorption processes for both pollutants were favorable, endothermic, and physical in nature. In the binary system, the presence of Cu(II) ions did not affect the adsorption capacity of ARS, while adsorption of Cu(II) was restricted in the presence of ARS. Furthermore, the synthesized beads could be regenerated through desorption of ARS using NaOH solution and could be reused up to five cycles. It can be concluded that removal of organic dyes (ARS) in the presence of inorganic cations (Cu(II)) can be accomplished using n-ZnO-impregnated chitosan beads as an eco-friendly alternative adsorbent.

3. Experimental

3.1. Materials

Chitosan (CS) (M.M. 10,000–300,000) was purchased from Acros Organics. A stock solution of 1000 mg L^{-1} of Cu(II) ions was prepared by dissolving 3.928 g of $CuSO_4.5H_2O$ (Merck) in distilled water containing 1 mL of conc. H_2SO_4 acid. Alizarin red S (ARS) was purchased from Riedel-de Häen AG, Germany. Sodium diethyldithiocarbamate was purchased from Loba Chemi, India. A stock solution containing 500 mg L^{-1} ARS was prepared by dissolving the required amount in distilled water. Working solutions were prepared daily by an appropriate dilution of the stock solution using distilled water. All other reagents used were of analytical reagent grade.

3.2. Synthesis

3.2.1. Synthesis of ZnO nanorods (n-ZnO)

The synthesis of n-ZnO was essentially based on the method of Gondal et al.[57] In a typical experiment, zinc nitrate and ammonium carbonate solutions were separately prepared by dissolving 40.0 g and 33.0 g, respectively, in 100 mL of distilled water. The zinc nitrate solution was added drop by drop into the ammonium carbonate solution, and the mixture was stirred continuously for 2 h. Then the formed precipitate was allowed to settle down for 24 h, filtered, and washed three times with distilled water and ethanol. The washed precipitate — the precursor for ZnO — was dried at 100 °C and calcined at 500 °C for 5 h in a programmable furnace to get the n-ZnO.

3.2.2. Synthesis of CS and CS-ZnO beads

The procedure employed was a modified version of the method given in the literature.[58] Typically, 1 g of the synthesized n-ZnO powder was dispersed and sonicated in 50 mL of 2% acetic acid, then added to a solution of 1 g of chitosan dissolved in 50 mL of 2% acetic acid. The mixture was stirred for 4 h until a clear solution was obtained. The formed solution was then dropped into a hot (70 °C) NaOH solution (20% w/v), where the drops turned immediately into white beads of CS-ZnO; these beads were kept in the solution at 60 °C for about 3 h. The wet gel beads were filtered, washed extensively with distilled water to remove any NaOH, and dried in an oven at 50 °C. For CS bead preparation, the same steps were repeated without n-ZnO addition.

3.3. Characterization

FTIR spectra were recorded on an FTIR spectrometer (FT-IR-6100 Jasco, Japan), using KBr pellets in the range of 4000–400 cm^{-1} at room temperature with spectral resolution 4 cm^{-1}. XRD studies were carried out using an X-ray diffractometer (X'Pert Pro, PANanalytical, the Netherlands) with Cu Kα radiation (λ = 0.15406 nm) in the 2θ range of 2° to 80°. The surface morphology of the beads was studied using a field emission scanning electron microscope (Quanta FEG 250, the Netherlands). The sample was coated with gold before SEM testing. Elemental composition was performed using an energy dispersive X-ray analyzer (X-flash Detector 410-M, the Netherlands) to obtain information on the content of n-ZnO in the synthesized beads. HR-TEM observation was carried out on a JEOL JEM-2100 Plus (USA) transmission electron microscope.

3.4. Adsorption experiments

Adsorption experiments were carried out using a batch mode. To study the effect of pH on the adsorption process, 0.1 g of the adsorbent was mixed with 50 mL of Cu(II) or ARS solution with initial concentration of 10 and 20 mg L^{-1}, respectively. The initial pH values of solutions were adjusted in the range of 2–10 using Thiel buffer. For adsorption kinetics studies, 50 mL of the Cu(II) (pH 6) or ARS (pH 2) solutions with initial concentration of 10 and 20 mg L^{-1}, respectively, were added to 0.1 g of adsorbent. In the adsorption isotherm studies, 0.1 g of the adsorbent was added to 50 mL of the Cu(II) or ARS solutions with an initial concentration of 10, 20, 30, 50, and 100 mg L^{-1} at the optimum pH for each. In the thermodynamic studies, 0.1 g of the adsorbent was added to 50 mL of Cu(II) or ARS solutions with initial concentrations 10 and 20 mg L^{-1}, respectively, at different temperatures. After equilibration, the concentration of the ARS was determined spectrophotometrically employing a Jasco 630V spectrophotometer at a wavelength of 420 nm, while copper was determined using the modified sodium diethyldithiocarbamate method.[59] The percentage of adsorption (%E) and q_e (mg g^{-1}) were calculated as follows:

$$\%E = \frac{C_o - C_e}{C_o} \times 100, \tag{15}$$

$$q_e = (C_o - C_e)\,\frac{V}{m}(\text{mg } g^{-1}), \tag{16}$$

where C_o and C_e are the initial and equilibrium concentrations of the solution (mg L^{-1}), respectively. V is the volume of the aqueous solution (L) and m is the mass of adsorbent in grams.

The stratification between the model-calculated values and the experimental results was explicated by the total mean error ($\epsilon\%$), which is the discrepancy between the experimental results and the calculated values:[60]

$$\epsilon\% = \frac{\sum_{i=1}^{n} |\,(q_{e(\exp.)} - q_{e(calc.)})\,|}{\sum_{i=1}^{n} q_{e(\exp.)}}. \tag{17}$$

A relatively low value of ε % specifies which model can be successfully used to describe the adsorption data.

3.5. Desorption and reusability studies

A static desorption process was performed by mixing 0.02 g of Cu(II)-loaded sorbent with 10 mL of 1 g L^{-1} EDTA solution and 0.02 g of ARS-loaded sorbent with 10 mL of 0.5 M NaOH. The released dye concentration was measured as mentioned above, while Cu(II) concentrations were determined using an atomic absorption spectrometer (AAnalyst 400, PerkinElmer) instead of the spectrophotometric method to avoid possible conflict due to the presence of EDTA. After desorption, the adsorbent was again used for readsorption of Cu(II) or ARS. Thus, adsorption/desorption cycles were repeated to establish the regeneration of the adsorbent, until there was a significant decrease in the adsorption efficiency.

3.6. Binary system studies

An amount of 0.1 g of the adsorbent was added to 50 mL of a solution mixture. A mixture series was prepared as a mixture of 10 mg L^{-1} Cu(II) with 10, 20, 30, 50, or 100 mg L^{-1} ARS at pH 2. After 48 h, the residual concentrations of Cu(II) and ARS were determined as mentioned previously in the adsorption experiments section.

Acknowledgments

The authors are grateful to the Faculty of Science, Helwan University (Egypt), for providing the necessary research facilities. The authors also thank the National Research Center for providing the usage of their equipment.

References

1. Batool, S.; Akib, S.; Ahmad, M.; Balkhair, K. S.; Ashraf, M. A. *J. Nanomater.* **2014**, *2014*, 864914.
2. Luna, L. A.; Silva, T. H.; Nogueira, R. F.; Kummrow, F.; Umbuzeiro, G. A. *J. Hazard. Mater.* **2014**, *276*, 332-338.
3. Barakat, M. A. *Arab. J. Chem.* **2011**, *4*, 361-377.
4. Nebagha, K. C.; Ziat, K.; Rghioui, L.; Khayet, M.; Saidi, M.; Aboumaria, K.; El Hourch, A.; Sebti, S. *J. Mater. Environ. Sci.* **2015**, *6*, 3022-3033.
5. Sacristán, D.; Peñarroya, B.; Recatalá, L. *Land Degrad. Dev.* **2015**, *26*, 587-595.
6. Eltaweel, Y. A.; Nassef, E. M.; Hazza, R. A. *World Environ.* **2014**, *4*, 199-205.
7. Abd El-Rahim, W. M.; Zaki, E. A. *Arab J. Biotech.* **2005**, *8*, 189 -200.
8. Wei, Y.; Gao, H. *J. Mater. Chem.* **2012**, *22*, 5715 -5722.
9. Gholivand, M. B.; Yamini, Y.; Dayeni, M.; Seidi, S.; Tahmasebi, E. *J. Environ. Chem. Eng.* **2015**, *3*, 529-540.
10. Fan, L.; Zhang, Y.; Li, X.; Luo, C.; Lu, F.; Qiu, H. *Colloids Surf. B* **2012**, *91*, 250-257.
11. Gautam, R. K.; Gautam, P. K.; Chattopadhyaya, M. C.; Pandey, J. D. *Sect. A Phys. Sci. Proc. Natl. Acad. Sci. India* **2014**, *84*, 495-504.
12. Visa, M.; Chelaru, A. M. *Appl. Surf. Sci.* **2014**, *303*, 14-22.
13. Sharma, R.; Kaith, B. S.; Kalia, S.; Pathania, D.; Kumar, A.; Sharma, N.; Street, R. M.; Schauer, C. *J. Environ. Manage.* **2015**, *162*, 37-45.
14. Qiao, H.; Zhou, Y.; Yu, F.; Wang, E.; Min, Y.; Huang, Q.; Pang, L.; Ma, T. *Chemosphere* **2015**, *141*, 297-303.
15. Al, E.; Güçlü, G.; İyim, T. B.; Emik, S.; Özgümüş, S. *J. Appl. Polym. Sci.* **2008**, *109*, 16-22.
16. Güçlü, G.; Keleş, S. *J. Appl. Polym. Sci.* **2007**, *106*, 2422-2426.

17. He, X.; Du, M.; Li, H.; Zhou, T. *Int. J. Biol. Macromol.* **2016**, *82*, 174-81.
18. Wu, F. C.; Tseng, R. L.; Juang, R. S. *Chem. Eng. J.* **2009**, *150*, 366-373.
19. Nawi, M. A.; Sabar, S.; Jawad, A. H.; Sheilatina ; Wan Ngah, W. S. *Biochem. Eng. J.* **2010**, *49*, 317-325.
20. Norranattrakul, P.; Siralertmukul, K.; Nuisin, R. *J. Met. Mater. Miner.* **2013**, *23*, 9-22.
21. Zhu, H.; Jiang, R.; Xiao, L.; Liu, L.; Cao, C.; Zeng, G. *Appl. Surf. Sci.* **2013**, *273*, 661-669.
22. Zhang, J.; Zhou, Q.; Ou, L. *J. Chem. Eng. Data* **2012**, *57*, 412-419.
23. Kumar, P. S.; Selvakumar, M.; Babu, S. G.; Jaganathan, S. K.; Karuthapandian, S.; Chattopadhyay, S. *RSC Adv.* **2015**, *5*, 57493-57501.
24. Travlou, N. A.; Kyzas, G. Z.; Lazaridis, N. K.; Deliyanni, E. A. *Chem. Eng. J.* **2013**, *217*, 256-265.
25. Kyzas, G. Z.; Travlou, N. A.; Deliyanni, E. A. *Colloids Surf. B* **2014**, *113*, 467-476.
26. Meyer, B.; Rabaa, H.; Marx, D. *Phys. Chem. Chem. Phys.* **2006**, *8*, 1513-1520.
27. Kikuchi, Y.; Qian, Q. R.; Machida, M.; Tatsumoto, H. *Carbon* **2006**, *44*, 195-202.
28. Lasheen, M. R.; El-Kholy, G.; Sharaby, C. M.; Elsherif, I. Y.; El-Wakeel, S. T. *Manage. Environ. Quality Int. J.* **2008**, *19*, 367-376.
29. Haldorai, Y.; Shim, J. *Compos. Interfaces* **2013**, *20*, 365-377.
30. Salehi, R.; Arami, M.; Mahmoodi, N. M.; Bahrami, H.; Khorramfar, S. *Colloids Surf. B* **2010**, *80*, 86-93.
31. Guo, M., Diao; P.; Cai, S. *J. Solid State Chem.* **2005**, *178*, 1864-1873.
32. Perelshtein, I.; Ruderman, E.; Perkas, N.; Tzanov, T.; Beddow, J.; Joyce, E.; Mason, T. J.; Blanes, M.; Mollá, K.; Patlolla, A. et al. *J. Mater. Chem. B* **2013**, *1*, 1968-1976.
33. Vicentini, D. S.; Smania, A. Jr; Laranjeira, M. C. M. *Mater. Sci. Eng. C* **2010**, *30*, 503-508.
34. Bhadra, P.; Mitra, M. K.; Das, G. C.; Dey, R.; Mukherjee, S. *Mater. Sci. Eng. C* **2011**, *31*, 929-937.
35. Joshi, K. M.; Shrivastava, V. S. *Int. J. Environ. Sci.* **2011**, *2*, 8-21.
36. El-Sigeny, S.; Mohamed, S. K.; Abou Taleb, M. F. *Polym. Compos.* **2014**, *35*, 2353-2364.
37. de Oliveira Brito, S. M.; Carvalho Brito, H. M.; Soares, L. F.; Azevedo, R. P. *J. Hazard. Mater.* **2010**, *174*, 84-92.
38. Schwarz, J. A.; Contescu, C. I. *Surfaces of Nanoparticles and Porous Materials;* Marcel Dekker: New York, NY, USA, 1999.
39. Rincón-Silva, N. G.; Moreno-Piraján, J. C.; Giraldo, L. *Adsorption* **2016**, *22*, 33-38.
40. Weber, W. J.; Morris, J. C. *J. Sanit. Eng. Div. Am. Soc. Civ. Eng.* **1963**, *89*, 31-59.
41. Yakout, S. M.; Elsherif, E. *Carbon Sci. Tech.* **2010**, *3*, 144-153.
42. Wu, F. C.; Tseng, R. L.; Juang, R. S. *J. Hazard. Mater.* **2000**, *73*, 63-75.
43. Hai, T.; Gui-Zhong, L.; You-Bin, Y.; Jian-Long, G. *Environ. Protec. Eng.* **2012**, *38*, 79-95.
44. Crank, J. *The Mathematics of Diffusion*; 1st ed. Oxford, UK: Clarendon Press, 1965.
45. Vijayaraghavan, K.; Padmesh, T. V. N.; Palanivelu, K.; Velan, M. *J. Hazard. Mater.* **2006**, *133*, 304-308.
46. Foo, K. Y.; Hameed, B. H. *Chem. Eng. J.* **2010**, *156*, 2-10.
47. Dabrowski, A. *Adv. Colloid Interface Sci.* **2001**, *93*, 135-224.
48. Freundlich, H. *Z. Phys. Chem.* **1907**, *57*, 385-470.
49. Adamson, A. W.; Gast, A. P. *Physical Chemistry of Surfaces*; 6th ed. Wiley- Interscience: New York, NY, USA, 1997.
50. Temkin, V.; Pyzhev, V. *Acta Physiochim. (URSS)* **1940**, *12*, 217-222.
51. García, E. R.; Medina, R. L.; Lozano, M. M.; Pérez, I. H.; Valero, M. J.; Franco, A. M. *Materials* **2014**, *7*, 8037-8057.

52. Vijayakumar, G.; Yoo, C. K.; Elango, K. G. P.; Dharmendirakumar, M. *Clean Soil Air Water* **2010**, *38*, 202-209.
53. Alkan, M.; Demirbas, O.; Celikapa, S.; Dogan, M *J. Hazard. Mater.* **2004**, *116*, 135-145.
54. Whitten, K. W.; Gailey, K. D.; Davis, R. E. *General Chemistry*; 4th ed. Saunders College Publishing: New York, NY, USA, 1992.
55. Chu, K. H. *J. Hazard. Mater.* **2002**, *90*, 77-95
56. Zolgharnein, J.; Choghaei, Z.; Bagtash, M.; Feshki, Sh.; Rastgordani, M.; Zolgharnein, P. *Des. Water Treat.* **2016**, *57*, 27672-27685.
57. Gondal, M. A.; Dastageer, M. A.; Khalil, A.; Hayat, K.; Yamani, Z. H. *J. Nanopart. Res.* **2011**, *13*, 3423-3430.
58. AbdElhady, M. M. *Int. J. Carbohydr. Chem.* **2012**, *2012*, 1-6.
59. Noll, C. A.; Betz, L. D. *Anal. Chem.* **1952**, *24*, 1894-1895.
60. Ali, O. I. M.; Osman, H. H.; Sayed, S. A.; Shalabi, M. E. H. *J. Hazard. Mater.* **2011**, *195*, 62-67.
61. Chen, J.; Zhang, W.; Li, X. *Polym. Bull.* **2016**, *73*, 1965-1984.
62. Wan, M. W.; Kan, C. C.; Rogel, B. D.; Dalida, M. L. P. *Carbohydr. Polym.* **2010**, *80*, 891-899.
63. Nuengmatcha, P.; Mahachai, R.; Chanthai, S. *Orient. J. Chem.* **2016**, *32*, 1399-1410.
64. Tsai, W. C.; de Luna, M. D. G.; Bermillo-Arriesgado, H. L. P.; Futalan, C. M.; Colades, J. I.; Wan, M. W. *Int. J. Polym. Sci.* **2016**, *2016*, 1608939.
65. Fu, F.; Gao, Z.; Gao, L.; Li, D. *Ind. Eng. Chem. Res.*, **2011**, *50*, 9712-9717.
66. Yantasee, W.; Lin, Y. H.; Fryxell, G. E.; Alford, K. L.; Busche, B. J.; Johnson, C. D. *Ind. Eng. Chem. Res.* **2004**, *43*, 2759-2764.